Meta-analysis of the melanoma miRNome identifies consensus signatures of progression and prognosis regulating metabolic plasticity and stress resistance

Borja Gómez-Cabañes[1,2,†], Helena Gómez-Martínez[1,†], Cristina Galiana-Roselló[1], Zoraida Andreu[3,4], Adolfo López[1,5], Nicole M Eskow[6], José A López-Guerrero[3,4,7], Marta R. Hidalgo[8], Eva Hernando[6,*], Francisco García-García[1,4,*]

Affiliations

[1]Computational Biomedicine Laboratory, Principe Felipe Research Centre (CIPF), Valencia, Spain.
[2]Programa de Doctorado en Biotecnología, Universitat Politècnica de València. Camí de Vera s/n, 46022 València, España.
[3]Laboratory of Molecular Biology, Foundation of the Valencian Institute of Oncology, Valencia, 46009, Spain.
[4]IVO-CIPF Joint Cancer Research Unit, Príncipe Felipe Research Center (CIPF), Av. Eduardo Primo Yúfera 3, Valencia, 46012, Spain.
[5]Joint unit in Artificial Intelligence and Biomedical Imaging FISABIO-CIPF, Foundation for the Promotion of Health and Biomedical Research of Valencia Region, Valencia, Spain.
[6]Department of Pathology, New York University Grossman School of Medicine, New York, US.
[7]Department of Pathology, Catholic University of Valencia, Valencia, Spain.
[8]Area of Applied Mathematics, Department of Applied Mathematics, Universidad de Valencia;Valencia, 46010, Spain.
[†]These authors contributed equally to this work

Corresponding authors:
Eva Hernando, Eva.Hernando-Monge@nyulangone.org
Francisco García-García, fgarcia@cipf.es

Keywords
Systematic review; meta-analysis; melanoma; transcriptomics; biomarkers; diagnosis; progression; microRNA; miRNome; metabolic plasticity; stress resistance

ABSTRACT

Melanoma incidence is rising, and accurate risk stratification remains challenging because of the molecular heterogeneity underlying disease progression. Specifically, the transition from benign nevi to malignant melanoma and the acquisition of the aggressive ulcerated phenotype represent critical barriers in clinical management that require novel biomarkers. In addition, there is a critical need for novel biomarkers to identify patients with primary melanoma who, despite complete surgical resection, remain at high risk of recurrence and would benefit from adjuvant therapy.

We applied an integrative systems biology approach to decipher the miRNA-dependent regulatory architecture of melanoma. Following PRISMA guidelines, we conducted a robust meta-analysis of six independent transcriptomic studies, overcoming inter-study heterogeneity. This was coupled with network inference algorithms to construct validated miRNA-mRNA interactomes and identify dynamic functional modules.

In the diagnostic scenario, we identified a consensus signature of 24 miRNAs. Network topology analysis revealed hsa-miR-142-5p as a master regulator that orchestrates the dismantling of the Oncogene-Induced Senescence (OIS) barriers by targeting CDK6, SIRT1, and TGFBR2. In the prognostic scenario (ulceration), we identified a specific "stress-adaptive" signature of 23 miRNAs. Notably, the upregulation of hsa-miR-223-3p emerged as a key driver of invasiveness by suppressing the motility-limiting tumor suppressor RHOB, while the concurrent loss of hsa-miR-200c and hsa-miR-489-3p may unleash Epithelial-Mesenchymal Transition (EMT) and EGFR-driven survival pathways.

Our study supports a double-switch mechanism where specific miRNA alterations first drive senescence escape and subsequently promote survival in the hypoxic ulcerated niche. These signatures offer robust

biomarkers for diagnosis and highlight the miR-142-5p/CDK6 and miR-223-3p/RHOB axes as potential therapeutic targets for precise intervention.

INTRODUCTION

Cutaneous melanoma represents the most lethal form of skin cancer, accounting for 80% of related mortalities despite comprising only 5% of cases (1,2). While the 5-year survival rate exceeds 98% for lesions confined to the epidermis (radial growth phase) (3), prognosis deteriorates precipitously once the tumor transitions to the vertical growth phase and invades the dermis (4). Crucially, the onset of ulceration serves as a clinical predictor of invasiveness and poor outcome, ranking as a top determinant for staging (5). However, current diagnostic challenges and the tumor's intrinsic biological heterogeneity often hinder early detection and precise risk stratification (6), underscoring the urgent need to elucidate the molecular checkpoints driving these critical transitions.

MicroRNAs (miRNAs) are short non-coding RNAs that regulate the expression of genes associated with numerous biological processes. They often exhibit disease-associated alterations in their expression profiles, which makes them a promising class of biomarkers for cancer diagnosis and prognosis (7–10). During melanoma and other cancer progressions, miRNA expression profiles are dysregulated (11,12). Previous studies have indicated that the expression of certain miRNAs, including hsa-miR-193a, hsa-miR-338, and hsa-miR-565, is reduced in BRAF-mutant melanoma. Additionally, low hsa-miR-191 and high hsa-miR-193b expression have been associated with poor survival outcomes (13). Furthermore, hsa-miR-4286 has been shown to modulate melanoma cell proliferation and apoptosis through multiple pathways (14). Alterations in miRNA expression profiles within melanoma tumor tissue have been associated with tumor formation, mutational status, and disease progression (15–17). However, significant research gaps persist regarding the reproducibility of these findings and the specific relationship between miRNA biomarkers and established clinical outcome predictors, demanding systematic cross-validation approaches.

We conducted a systematic review and meta-analysis strictly adhering to the Preferred Reporting Items for Systematic Reviews and Meta-Analyses (PRISMA) guidelines (18). This integrative computational approach, which evaluates all published miRNA expression datasets in melanoma, generates a consensus miRNA signature that clarifies the underlying regulatory processes, and supports the development of new diagnostic and treatment strategies. We identified a diagnostic core signature driven by hsa-miR-1973 and hsa-miR-142-5p among twenty-four differentially expressed miRNAs, which exposes molecular mechanisms of melanoma genesis, specifically regarding senescence escape, and may serve as clinical biomarkers. Additionally, a miRNA signature of twenty-three differentially expressed miRNA, with the hsa-miR-223-3p/hsa-miR-200c axis emerging as an indicator of ulceration and aggressive phenotype, potentially by orchestrating metabolic adaptation and anoikis resistance. An extensive in silico characterization of these miRNA signatures was conducted, providing insight into their biological role and clinical relevance in melanoma diagnosis and prognosis.

RESULTS

Systematic review and meta-analysis of miRNA studies

Our systematic review initially identified a total of 54 studies from the Gene Expression Omnibus (GEO) and ArrayExpress (AE) databases. In accordance with the established inclusion criteria, six studies were selected for inclusion in our analysis (**Figure 1** depicts the complete study selection process).

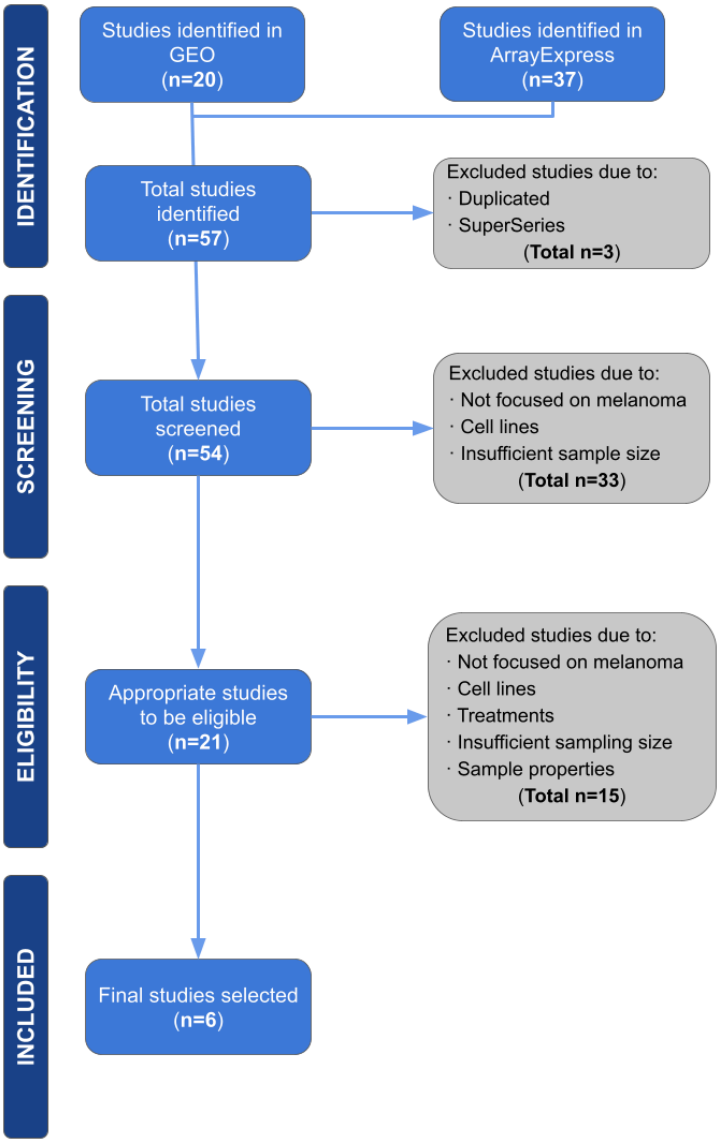

Figure 1. Prisma diagram of the systematic review.

These six studies were categorized into two different clinical "scenarios": i) diagnostic, which involved a comparison between primary cutaneous melanoma and benign nevi (PM vs. BN); and ii) prognostic, which involved a comparison between ulcerated melanoma and non-ulcerated melanoma (UM vs. NUM). The research incorporated studies published between 2010 and 2023, comprising a total cohort of 303 subjects, with miRNA expression detected within the skin tissue samples of these patients. The specific scenarios subjected to analysis, along with the corresponding number of differentially expressed miRNAs identified in

each study, are summarized in **Table S1** and **Table S2**, respectively. Subsequent meta-analysis of these expression signatures yielded a consensus set of significantly differentially expressed miRNAs pertinent to both diagnostic and prognostic contexts (**Table 1** and **Table S3**).

In the diagnostic scenario, a meta-analysis of 1,127 miRNAs identified 24 differentially expressed miRNAs, comprising 11 upregulated and 13 downregulated in PM. In the prognostic scenario, 23 differentially expressed miRNAs were identified from a total of 1,327 miRNAs, comprising 7 upregulated in UM and 16 downregulated in UM. Three miRNAs exhibited identical patterns of differential expression in both scenarios (PM vs BN and UM vs NUM). Specifically, hsa-miR-203 and hsa-miR-205 were found to be downregulated, while hsa-miR-21 was identified as an upregulated miRNA. The complete results for significant miRNAs are presented in **Table 1**.

We performed an orthogonal cross-validation of our severity signature using an independent dataset from the InterMEL consortium (19), which evaluated miRNA associations with ulceration in a large cohort of melanoma patients via NanoString profiling. To avoid background bias, we restricted our comparative analysis to the universe of 125 miRNAs consistently detected in the InterMEL cohort. Within this defined background, our meta-analysis identified 9 significant miRNAs (hsa-miR-451, hsa-miR-21, hsa-miR-200c, hsa-miR-223-3p, hsa-miR-203, hsa-miR-205, hsa-miR-363-3p, hsa-miR-135b-5p, hsa-miR-29a, hsa-miR-324-5p). This concordant directionality across independent technological platforms confirms that our consensus signature captures robust biological drivers of the ulcerated phenotype.

Table 1. Significant differentially expressed miRNAs identified by random-effects meta-analysis in diagnostic and prognostic scenarios. Data represent the consensus signatures for the Primary Melanoma vs. Benign Nevi (Diagnostic) and Ulcerated vs. Non-Ulcerated Melanoma (prognostic) comparisons. For each miRNA, the combined log2

fold-change (logFC) and the adjusted p-value are reported. Selection criteria for significance were defined as an adjusted p-value < 0.05 and an absolute logFC > 0.5.

Primary melanoma vs. Benign nevus			Ulcerated vs. Non-ulcerated		
miRNA	**logFC**	**adjusted p-value**	**miRNA**	**logFC**	**adjusted p-value**
hsa-miR-1973	3.556	0.0002	hsa-miR-223-3p	1.494	0.0070
hsa-miR-3648	3.340	0.0002	hsa-miR-196b-5p	1.351	0.0370
hsa-miR-3156-5p	3.072	0.0120	hsa-miR-135b-5p	1.262	0.0240
hsa-miR-3911	1.926	0.0040	hsa-miR-363-3p	1.195	0.0210
hsa-miR-21	1.776	0.0002	hsa-miR-451	1.049	0.0001
hsa-miR-3610	1.275	0.0380	hsa-miR-21	0.788	0.0010
hsa-miR-3138	1.274	0.0380	hsa-miR-29a	0.526	0.0390
hsa-miR-3195	1.156	0.0150	hsa-miR-200c	-0.501	0.0020
hsa-miR-3132	0.999	0.0380	hsa-miR-5010-5p	-0.511	0.0480
hsa-miR-142-5p	0.814	0.0020	hsa-miR-301a-5p	-0.515	0.0240
hsa-miR-22	0.754	0.0380	hsa-miR-450a-2-3p	-0.539	0.0390
hsa-miR-23a	-0.561	0.0380	hsa-miR-580-3p	-0.542	0.0480
hsa-miR-30c	-0.579	0.0190	hsa-miR-381-5p	-0.545	0.0400
hsa-let-7d	-0.632	0.0020	hsa-miR-203	-0.561	0.0190
hsa-let-7c	-0.646	0.0380	hsa-miR-487b-5p	-0.590	0.0480
hsa-miR-193b	-0.747	0.0002	hsa-miR-205	-0.593	0.0190
hsa-miR-508-3p	-1.040	0.0002	hsa-miR-552-3p	-0.597	0.0390
hsa-miR-509-3p	-1.305	0.0002	hsa-miR-499a-5p	-0.633	0.0030
hsa-miR-23b	-1.323	0.0002	hsa-miR-518e-3p	-0.649	0.0480
hsa-miR-203	-1.368	0.0160	hsa-miR-489-3p	-0.659	0.0480
hsa-miR-205	-1.571	0.0020	hsa-miR-133a-5p	-0.667	0.0190
hsa-miR-100	-1.700	0.0002	hsa-miR-624-3p	-0.669	0.0480
hsa-miR-101	-1.785	0.0002	hsa-miR-376c-5p	-0.749	0.0260
hsa-miR-211	-1.956	0.0080			

Functional *in silico* characterization of miRNA target genes

To characterize the functional impact of the meta-analyzed miRNAs, we performed a comprehensive enrichment analysis of their downstream target gene set, integrating biological annotations from Gene Ontology (GO-BP) and Reactome pathways. The diagnostic scenario yielded 15,684 unique target genes, while the prognostic scenario encompassed 20,150 targets included in the functional analysis.

Biological process analysis unveils survival strategies and microenvironment adaptation in primary melanoma

A Gene Set Analysis (GSA) on the GO-BP ontology was performed based on the complete miRNA-regulated transcriptomic profile for both scenarios. Within the diagnostic scenario, the fifteen GO-BP terms most significantly enriched in primary melanoma (**Figure 2A**) are dominated by mechanisms of mRNA stability and degradation via deadenylation and 3'UTR regulation. Furthermore, metabolic reprogramming, including alterations in glycolysis and the insulin pathway, suggests a metabolic reprogramming required for tumor

growth. Finally, perturbations in DNA repair, maintenance, and G1 phase regulation point towards genomic instability and proliferation. Comprehensive enrichment results are detailed in **Table S4**.

Given the substantial number of GO-BP terms significantly enriched in primary melanoma, semantic clustering was performed to distill the complex landscape of the diagnostic scenario. This analysis revealed five distinct functional clusters (**Figure 2B; Table S4**). The largest, Cluster 1, centers on mRNA metabolism and genetic information processing at transcriptional, post-transcriptional, and post-translational levels, underscoring the critical importance of gene regulation in this context. Cluster 4 highlights cell cycle dysregulation, particularly at the G1/S transition and DNA damage checkpoints (G1 and G2). These perturbations suggest a genomic instability, a theme intimately linked to Cluster 2, which aggregates apoptotic mechanisms driven by DNA damage and mitochondrial oxidative stress, alongside disruptions in growth factor and hormone signaling pathways. Concurrently, Cluster 3 captures alterations in differentiation and angiogenesis, encompassing tissue morphogenesis and endothelial cell migration. These tissue remodeling processes coincide with Cluster 5, which orchestrates cellular organization through vesicle and nuclear restructuring, membrane dynamics, and the regulation of cell adhesion and the actin cytoskeleton.

To dissect the functional topology of the processes enriched in primary melanoma, we constructed a term similarity network that reorganized the functional landscape into eight distinct modules that mirror the semantic clusters (**Figure 2C**). Connectivity patterns revealed a dichotomy between a highly integrated regulatory core and discrete effector modules. The "Apoptosis", "Cell Cycle", "Protein Phosphorylation", and "Post-transcriptional Regulation" modules exhibit a dense degree of internal and external connectivity. This connectivity pattern suggests close functional coupling between gene regulation, cell cycle checkpoints, and survival signaling in the malignant state. In contrast, "Response to External Stimuli", "Protein Organization", "Adhesion", and "Development and morphogenesis" display limited connectivity, appearing as independent, specialized functional units governing structural remodeling and microenvironmental adaptation.

Stress-induced epithelial reorganization and cell adhesion disruption characterize the ulcerated phenotype

Having established the functional architecture associated with the onset of primary melanoma, we next applied this integrative workflow to dissect potential mechanisms underlying melanoma ulceration. The *in silico* functional analysis comparing ulcerated and non-ulcerated tumors (**Figure S1**) reveals a transcriptome shaped by cellular stress and structural instability.

Among the top fifteen GO-BP terms enriched in ulcerated melanoma (**Figure S1A**), mechanisms of mRNA stability and RNA metabolism predominate, suggesting a high demand for rapid post-transcriptional adaptation. Comprehensive enrichment results are detailed in **Table S5**. Concurrently, processes governing cellular architecture, specifically adherens junction assembly and cell cycle regulation, are significantly altered, alongside robust DNA damage and stress response signatures. Semantic clustering (**Figure S1B, Table S5**) deconvoluted this complex landscape into distinct functional clusters. Cluster 1 highlights the central role of mRNA processing and post-transcriptional regulation. Notably, the phenotype is driven by Cluster 3, which orchestrates a multidimensional stress response to both internal insults (ROS, ER overload) and external signals (TGF-β, Wnt, TNF). This stress state is functionally coupled to Cluster 5, which aggregates mitochondrial apoptosis and DNA damage responses. These upstream regulatory events converge on Cluster 7, characterized by dysregulated cell-matrix adhesion. Underlying this loss of integrity, Cluster 4 reveals profound reorganization of intracellular transport and protein localization, supporting the epithelial remodelling and vascularization processes identified in Cluster 2.

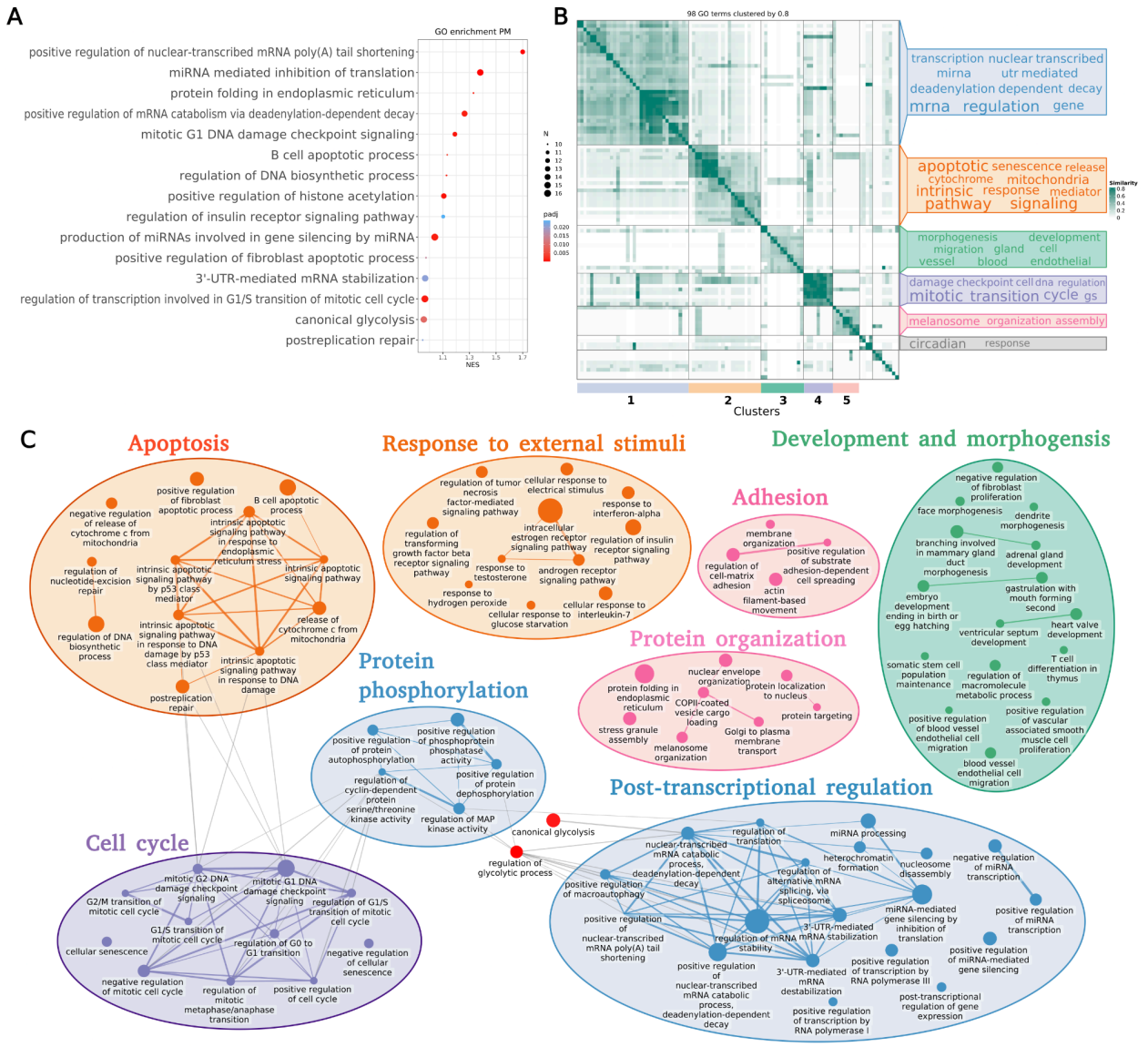

Figure 2. Functional landscape of the diagnostic miRNA signature in primary melanoma. (A) Dot plot illustrating the top fifteen GO-BP processes most significantly enriched in primary melanoma compared to benign nevi. The x-axis represents the Normalized Enrichment Score (NES); dot size and color indicate the gene set size and adjusted p-value, respectively. (**B**) **Semantic similarity matrix of all significant GO-BP terms enriched in primary melanoma.** The intensity indicates the degree of semantic similarity. Distinct functional clusters are identified on the axes and summarized by word clouds on the right. (**C**) **Functional network of processes enriched in primary melanoma.** Nodes represent GO-BP terms, with size proportional to statistical significance (adjusted p-value). Edges denote gene overlap between terms, with thickness proportional to the degree of similarity. Nodes are colored according to the semantic clusters defined in (**B**) and grouped into functional modules labeled by their representative biological activity. Only GO-BPs with a logFC cutoff > 0.5 were included.

To elucidate the hierarchy of these processes, we built a term similarity network (**Figure S1C**). The resulting topology reveals strong interconnectivity among mRNA stability, epigenetic regulation, and splicing modules, reflecting a coordinated reprogramming of the genetic information flow. A central "Stress-Response" module links the cell cycle checkpoints with mitochondrial apoptosis and internal stress sensing, suggesting that the ulcerated phenotype involves a balance between survival and cell death signals. Notably, the "Adhesion" and "Vesicular transport" modules are functionally linked to this stress-response core. This architecture suggests that ulceration is not merely a passive necrosis, but involves an active stress-adaptive program associated with the destabilization of cell adhesion and tissue cohesion machinery.

Reactome profiling implicates disruption of oncogene-induced senescence and TGF-β signaling in early melanomagenesis

To delineate the specific signaling cascades driving melanoma progression, we employed Reactome pathway annotation, focusing primarily on pathways enriched in primary melanoma given the limited number of downregulated sets. This analysis generated a hierarchical functional signature organized into seven biological Pathways Blocks (PB) (**Figure 3**). PB were defined based on functional grouping of Reactome pathways: 1- Genetic information control and processing, 2- Metabolic processes, 3- Cell signaling and responses, 4- Transport and structural organization, 5- Cell survival and death, 6- Development and maintenance, and 7- Immune response. A more comprehensive functional profile at sub-pathway blocks (PB.S) level is detailed for each comparison in **Table S5** and **Table S6** respectively.

Reactome profiling of the diagnostic scenario (fully detailed in **Table S6**) suggests the disruption of Oncogene-Induced Senescence (OIS) as a central event differentiating primary melanoma from benign nevi. This hallmark is molecularly defined by widespread alterations in cell cycle checkpoints, specifically the DNA damage-dependent control of G1/S transition mediated by the RB1/E2F1 axis and CDK complexes (**PB1.1, PB3.3**). These defects are compounded by dysregulation of the p53 pathway in response to checkpoint violation (**PB1.3**), creating a permissive environment for proliferation. Mechanistically, enrichment pattern indicates coupling between senescence pathways and stress response signaling (**PB3.1-2**), where perturbations in PTEN and RAF regulation converge with a defective RB1 tumor suppressor axis. Metabolic rewiring sustains this transformation by driving SUMOylation-dependent post-translational modifications and enhancing mRNA capping processing (**PB2.2-3**), alongside specific disruptions in nitric oxide metabolism (NOS3) and BAD-mediated apoptotic signaling (**PB2.1, PB5.1**). Concurrently, significant perturbations in Rho GTPase signaling underscore an early acquisition of cytoskeletal plasticity and motility potential (**PB3.2**). Notably, the most extensive pathway alterations converge on TGF-β and SMAD signaling (**PB3.2**), suggesting the disruption of TGF-β cytostatic signaling as a driver of early melanomagenesis.

Dysregulated Rho GTPase signaling and angiogenic cascades are enriched aggressive ulcerated phenotype

While the diagnostic profile underscored the evasion of suppressive checkpoints, we asked whether the aggressive ulcerated phenotype may rely on distinct signaling networks. Reactome pathway analysis revealed a landscape defined by invasive signaling and metabolic stress adaptation (fully detailed in **Table S7**). Significant alterations in cell cycle regulation and DNA repair, including p53-related mechanisms (**PB1.1-1.2-1.3**), suggest compromised genomic integrity and heightened replicative stress. These alterations are compounded by widespread metabolic rewiring, spanning lipid and carbohydrate metabolism (**PB2.1**), alongside critical disruptions in RNA processing and protein quality control (**PB2.2-3**). Notably, the enrichment of protein folding and SUMOylation pathways highlights a cellular state under acute proteotoxic stress, functionally linked to the cellular responses to external stimuli identified in **PB3.1**.

We observed extensive perturbation in signal transduction in ulcerated melanoma, dominated by Rho GTPase and receptor tyrosine kinase (RTK) signaling (**PB3.2**). These pathways drive cytoskeletal dynamics essential for invasion and are intimately associated with altered cell-cell communication, extracellular matrix interactions, and death receptor signaling (**PB3.2-3, PB4.3**), thereby linking the loss of tissue integrity with resistance to apoptotic mechanisms such as anoikis. Furthermore, the simultaneous deregulation of autophagy, regulated necrosis, and apoptosis (**PB5.1-2**) suggests a plasticity that enhances survival during dissemination. Concurrently, the activation of hemostasis and platelet signaling pathways points to enrichment of pro-angiogenic signaling (**PB7.1**), supporting the tumor's dependence on neovascularization. Finally, the profound dysregulation of innate and adaptive immune pathways (**PB7.2**) reflects a chronic inflammatory and immunosuppressive microenvironment, which, together with altered growth factor signaling (**PB3.2-3**) and developmental processes (**PB6.2**), fuels the progression of the high-risk ulcerated melanoma.

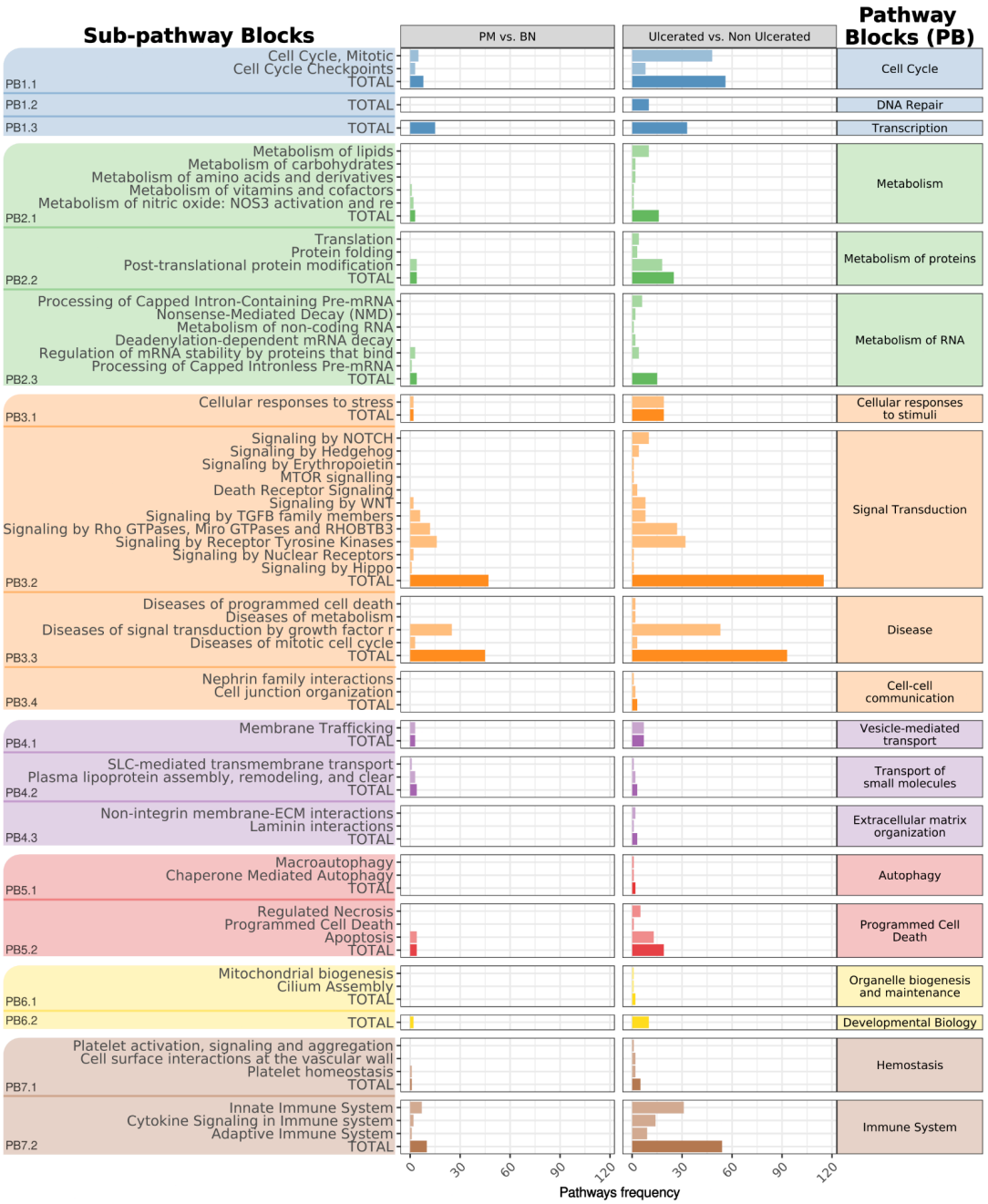

Figure 3. Hierarchical functional pathways signature of the diagnostic and prognostic scenarios. The bar plot displays the frequency distribution of significant Reactome pathways enriched in primary and ulcerated melanoma, categorized into seven distinct **Pathway Blocks (PB)** (right Y-axis, color-coded). Each block groups Top-level pathways, which are further resolved into specific sub-pathways (left Y-axis) detailing precise molecular events. The "TOTAL" bar represents the aggregate count of significant events within each top-level category. The X-axis indicates the number of significant pathways identified in the **Diagnostic (Primary Melanoma vs. Benign Nevi)** and **Prognostic (Ulcerated vs. Non-Ulcerated)** contrasts, allowing for a direct comparison of the functional load associated with tumor initiation versus progression.

Network analysis of validated miRNA targets reveals regulatory architecture in melanomagenesis and ulceration

To further interpret the functional consequences of the identified miRNA signatures, we constructed Protein-Protein Interaction (PPI) networks restricted to experimentally validated target genes with

confirmed skin tissue expression. This approach allowed us to map how the dysregulated miRNA landscape remodels the melanoma molecular landscape.

miRNA-driven suppression of senescence and metabolic regulators in primary melanoma

In the diagnostic scenario (Primary Melanoma vs. Benign Nevi), the integration of differentially expressed miRNAs with their previously validated targets revealed a highly interconnected PPI network characterized by a dense central cluster of 31 genes (p-value: 2.46e-10) (**Figure 4A; Table S8**). This topology suggests that the transition to malignancy is associated with the coordinated disruption of specific functional dynamics rather than isolated gene events. The network architecture resolved into three modules that mechanistically define early melanomagenesis.

First, OIS and senescence-associated secretory phenotype (SASP) (Module 1) emerged as a major target of miRNA-mediated regulation. This module comprises critical cell cycle and survival regulators, including PTEN, TP53INP1, CDK6, CCND1, and CASP2, alongside key mediators of the SASP such as SOCS1 and IL6ST. Second, the network highlighted a module integrating Proliferation and Epithelial-Mesenchymal Transition (EMT) (Module 2). This cluster connects the TGF-β signaling axis (TGFBR2, SMAD3) with drivers of mesenchymal plasticity (ZEB1, RAC1) and migratory capability (ITGAV, KIT, ABL2). The connectivity between these factors links the acquisition of invasive potential with the alteration of growth factor signaling pathways. Third, Metabolic Reprogramming (Module 3) was identified as a distinct functional block, centered on metabolic sensors including SIRT1, HIF1A, and MCL1, as well as ENPP1 and NFE2L2. The presence of HIF1A and SIRT1 as hubs within this module suggests metabolic adaptation to hypoxic or oxidative stress.

Notably, the regulatory network analysis (**Figure 4B**) identified hsa-miR-142-5p as a multifunctional master regulator, extending its repressive control across all three functional modules by simultaneously targeting SIRT1, HIF1A, TGFBR2, RAC1, and CDK6. This convergence positions hsa-miR-142-5p as a potential regulatory node that integrates metabolic rewiring with the evasion of senescence and the onset of motility. Additionally, the analysis highlighted hsa-miR-3648, hsa-miR-3138, and hsa-miR-3911 as modulators of the OIS machinery, while hsa-miR-3911 further acts as a dual regulator bridging EMT and metabolic control in conjunction with hsa-miR-3132 and hsa-miR-3156-5p.

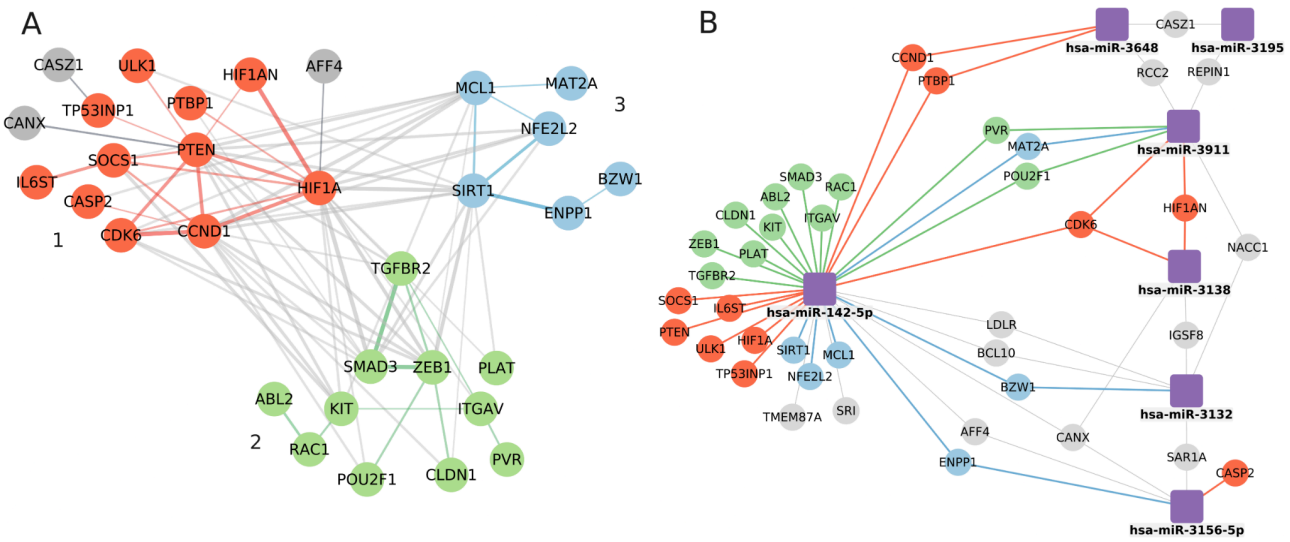

Figure 4. Integrated interaction and regulatory networks linked to early melanomagenesis. (A) Protein-Protein Interaction (PPI) network of validated target genes from miRNAs upregulated in primary melanoma. Nodes represent target genes, while edge thickness indicates the interaction confidence score. The network topology resolves into three distinct dynamic regulatory modules (color-coded): 1) Oncogene-Induced Senescence (OIS) and

senescence-associated secretory phenotype (SASP); 2) Proliferation and Epithelial-Mesenchymal Transition (EMT); and 3) Metabolic reprogramming. Unconnected nodes were excluded to highlight the core interactome. **(B) miRNA-Target Regulatory Network**. Square nodes represent miRNAs upregulated in primary melanoma, whereas circular nodes correspond to their target genes. Node colors indicate the functional modules defined in (A), while gray nodes refer to targets with lower connectivity or distinct functional roles.

Upregulated miRNAs in ulcerated melanoma target cell cycle and stress response checkpoints

In the prognostic scenario (Ulcerated vs. Non-Ulcerated), the PPI network analysis of targets of miRNA upregulated in ulcerated melanoma unveiled a dense and highly integrated architecture of 137 genes (p-value: 1.0e-16), characterized by the simultaneous targeting of cell growth and surveillance machinery (**Figure 5A; Table S9**). The network topology is defined by specific functional modules. We observed a physical connectivity between cell cycle regulators (CDK4, CDK6, E2F1) and key sensors of genotoxic and metabolic stress (ATM, HIF1A, PTEN, MDM2). This topology supports a molecular integration of proliferative signaling and stress checkpoints, suggesting that the ulcerated phenotype relies on a coordinated response to sustain growth under adverse conditions. The network highlights a high degree of regulation on genes related to cell-matrix adhesion and cytoskeletal stability, identifying ICAM1, STMN1, and crucially, RHOB as central nodes. In the immune module, STAT3 and IL6 emerged as hub genes acting as inter-module connectors.

The regulatory network analysis (**Figure 5B**) places hsa-miR-223-3p at the center of this network. This miRNA exhibits the highest connectivity, directly targeting RHOB, ICAM1, and STMN1, alongside cell cycle modulators. Additionally, the analysis revealed that hsa-miR-363-3p targets PTEN and BCL2L11, while hsa-miR-196b-5p and hsa-miR-135b-5p converge to co-regulate a specific sub-network centering on HIF1A.

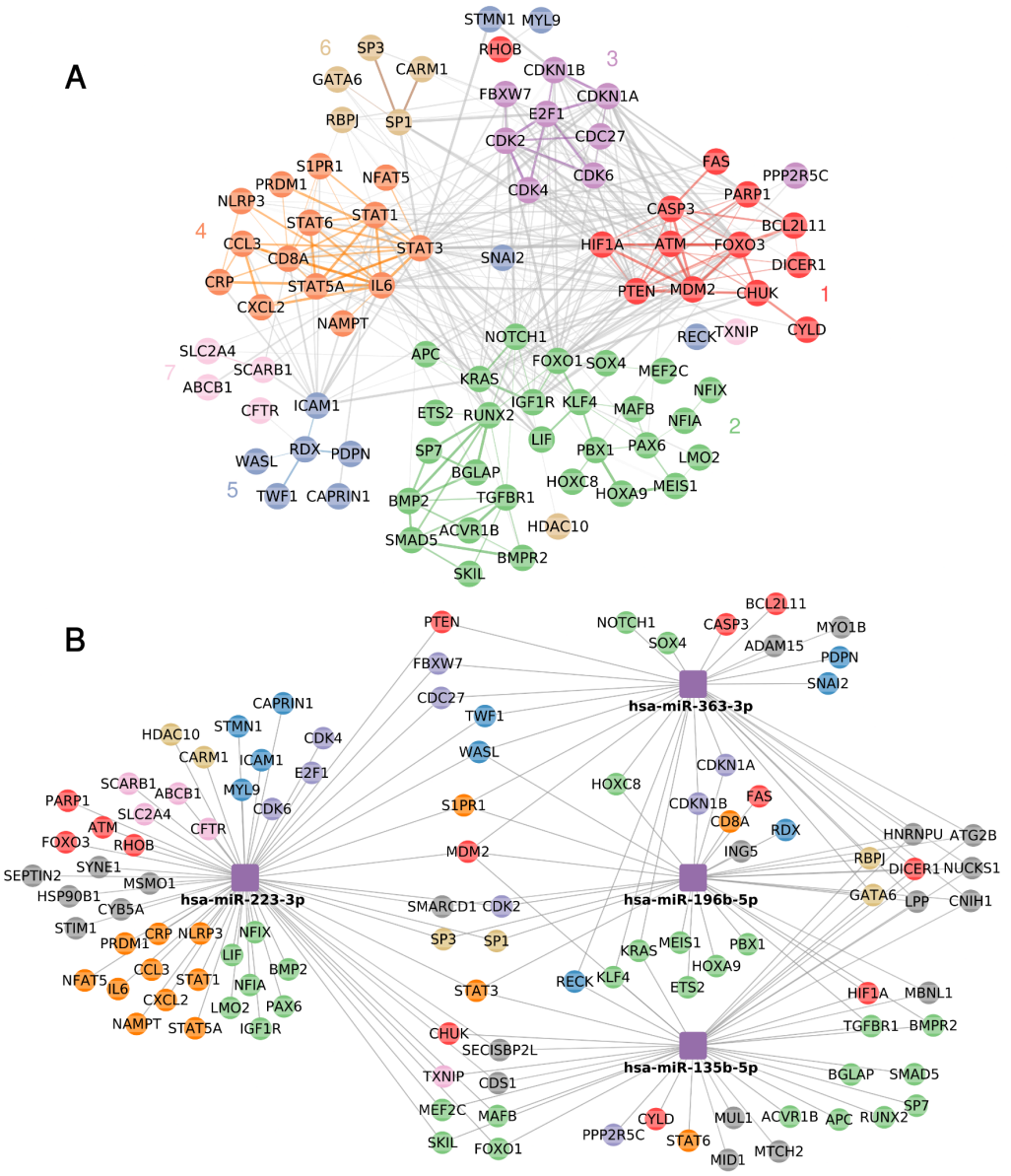

Figure 5. Integrated interaction and regulatory networks characterizing the ulcerated melanoma phenotype. (A) Protein-Protein Interaction (PPI) network of validated target genes of miRNAs upregulated in ulcerated melanoma. Nodes represent target genes, while edge thickness indicates the interaction confidence score. Edges are colored to denote intragroup (matching node color) or intergroup (gray) connections. The network topology resolves into seven distinct dynamic regulatory modules (color-coded): 1) Stress and cell death; 2) Cellular differentiation and proliferation; 3) Cell cycle; 4) Immune system; 5) Mobility and adhesion; 6) Signal transduction and genome maintenance; and 7) Metabolism. Unconnected nodes were excluded. **(B) miRNA-Target Regulatory Network**. Square nodes represent miRNAs upregulated in ulcerated melanoma, whereas circular nodes correspond to their target genes. Node colors indicate the functional modules defined in (A), while gray nodes refer to targets with lower connectivity or distinct functional roles.

Ulcerated melanoma is associated with loss of miRNA-mediated repression of growth factor signaling networks

Conversely, the analysis of downregulated miRNAs in ulcerated melanoma yielded a distinct, highly interconnected network of 50 genes (p-value: 1.0e-16) (**Figure S2A; Table S10**). The topological organization reveals a dominant core related to growth and signaling (Module 2), characterized by a dense cluster of receptor RTKs and signal transducers, including ERBB2, IGF1R, EGFR, PIK3R2, and SMAD4. This central signaling hub exhibits direct interactions with the cell motility and cytoskeleton cluster (Module 5), bridging

growth signals with EMT drivers such as SNAI2 and TWIST1. The network also integrates regulators of the cell cycle (Module 3), specifically FOXM1 and CDKN1A, and stress response mediators (Module 1) such as FOXO4 and PDCD4.

The regulatory network analysis (**Figure S2B**) highlights a hierarchical structure where hsa-miR-489-3p and hsa-miR-499a-5p emerge as the most influential nodes. These miRNAs display the highest connectivity, particularly targeting the growth factor receptor module. Specifically, hsa-miR-489-3p, in conjunction with hsa-miR-552-3p, hsa-miR-5010-5p, and hsa-miR-133a-5p, forms a regulatory cluster converging on growth-related targets. Additionally, hsa-miR-376c-5p may cooperate with the central regulators to modulate the stress response machinery.

DISCUSSION

Melanoma progression requires overcoming two distinct barriers: the intrinsic arrest of OIS in nevi and the extrinsic stress of the ulcerated microenvironment. Our integrated miRNA-mRNA analysis suggests a hierarchical structure, identifying hsa-miR-142-5p as a potential regulator of the initial senescence escape. We propose that this early deregulation establishes the permissive landscape required for subsequent metabolic and structural adaptations in ulcerated tumors, highlighting a specific miRNA-driven axis for risk stratification.

The functional architecture of the diagnostic scenario, visualized in **Figure 2** and **Figure 3** (and fully detailed in **Table S4** and **Table S6**), suggests that dysregulation of the G1 checkpoint and DNA repair machinery triggers aberrant cell fate decisions—quiescence, senescence, or apoptosis—involving TP53INP1-dependent signaling nodes following irreparable DNA damage (**Cluster 4; PB1.3, PB3.3**) (20,21). These molecular events underpin OIS and initiate the senescence-associated secretory phenotype (SASP), as substantiated by our *in silico* functional analysis (**PB3.1**) (22,23). Notably, while transient SASP activity mediates tissue repair and immune clearance, its chronic persistence paradoxically fuels tumor progression by inducing cellular plasticity and remodeling the microenvironment (**PB3.2**) (24,25). We identified hsa-miR-142-5p as a central node potentially connecting OIS escape with melanoma progression. Network analysis (**Figure 4**) suggests that this miRNA converges on critical effectors of the DNA damage response, specifically TP53INP1, and on master regulators of metabolism and survival, including SIRT1, HIF1A, and PTEN (26–28). This pleiotropic regulation is supported by the functional enrichment of metabolic stress and p53 signaling pathways observed in our data (**Cluster 2; PB3.2, PB1.3**). These findings suggest that hsa-miR-142-5p may modulate cellular fate by post-transcriptionally balancing metabolic rewiring and proliferation under oncogenic stress.

Mechanistically, OIS relies on a stable G1–S arrest mediated by the CDK4/6–RB axis (**Cluster 4; PB1.1**) (29,30). Our network suggests a coordinated regulation where hsa-miR-142-5p, alongside hsa-miR-3911 and hsa-miR-3138, converges on CDK6, while hsa-miR-3648 targets CCND1. Regulation of these cyclins and CDKs may fine-tune cell cycle progression under oncogenic stress, rather than forcing complete arrest. Crucially, hsa-miR-142-5p bridges this cycle modulation with the secretory phenotype by targeting ULK1 and signaling via IL6ST (Figure 2C). Since autophagy supplies the metabolic substrates required for robust SASP production (23,31), this miRNA-driven axis may regulate the critical balance between tumor-suppressive clearance and tumor-promoting inflammation driven by chronic IL-6 exposure (31,32). Furthermore, our data implicate hsa-miR-142-5p in dismantling the TGF-β/SMAD tumor-suppressive axis by directly targeting TGFBR2 and SMAD3. While physiological TGF-β signaling enforces cytostasis in early lesions (33), the suppression of these core components suggests a mechanism for acquiring insensitivity to antiproliferative cues (34). This disruption aligns with the established role of defective TGF-β signaling in supporting sustained oncogenic signaling and immune evasion (**Clusters 1-2; PB3.2-3**) (34,35). Our network topology further suggests that hsa-miR-142-5p supports the metabolic plasticity required for invasiveness by integrating HIF1A and PTEN with SIRT1 (36,37). SIRT1 emerges as a potentially critical node, as it governs glycolipid reprogramming and actively suppresses senescence in melanoma cells (38,39). The targeting of

SIRT1 by hsa-miR-142-5p, alongside the modulation of the ZEB1 axis—which drives dedifferentiation and confers anoikis resistance via PI3K/Akt signaling (**Cluster 3**) (40)—indicates a complex regulatory mechanism. We propose that this miRNA may act as a "metabolic switch," balancing the suppression of senescence barriers with the activation of survival pathways essential for early dissemination.

Complementing its central role, the network integrates a functional switch characterized by the downregulation of hsa-miR-205 and the concurrent upregulation of hsa-miR-21. The loss of hsa-miR-205 may relieve ZEB1 repression to drive Epithelial-Mesenchymal Transition (EMT) (41), while hsa-miR-21 simultaneously targets PTEN to sustain AKT/ERK signaling (42). This latter axis mechanistically couples EMT with metabolic reprogramming by promoting HIF-1α expression and the hypoxic response (**Cluster 2; P3.2**) (43). Collectively, hsa-miR-142-5p functions as the nodal integrator of this network, fine-tuning pathway outputs to enable senescence escape and metastatic progression.

Beyond initial transformation, the clinical progression toward aggressive ulcerated phenotypes introduces severe nutrient deprivation and matrix detachment. The functional landscape of this transition, visualized in **Figure S1** and **Figure 3** (and detailed in **Table S5** and **Table S7**), suggests that, while the resulting metabolic crisis and reactive oxygen species (ROS) accumulation typically drive anoikis (40,44,45)—consistent with our *in silico* functional data (**Cluster 5**)—ulcerated cells appear to exploit moderate oxidative stress to paradoxically promote survival via HIF1A signaling (**Cluster 3; PB3.2**) (46,47). To counteract bioenergetic collapse, ulcerated melanoma cells likely activate autophagy (**Cluster 1; PB5.1**) (48,49). Our data suggest that hsa-miR-196b-5p and hsa-miR-135b-5p orchestrate this reprogramming by co-regulating HIF1A and the autophagy-related gene ATG2B (**Figure 5B; PB3.1**), revealing a novel miRNA-mediated mechanism for sustaining anchorage-independent survival in the ulcerated microenvironment.

Reinforcing these intracellular adaptations, the sustained regulation of EGFR and ERBB2—modulated by hsa-miR-133a-5p, hsa-miR-301a-5p, hsa-miR-489-3p, and hsa-miR-552-3p (Figure 5B)—provides essential survival signals (44,50). Functionally, these receptors activate MAPK and PI3K/Akt pathways to suppress the pro-apoptotic protein BCL2L11 (Bim) (51) and rescue cells from anoikis by maintaining ATP levels (**Clusters 3-5; PB3.2-3**) (44,46,51). This resistant phenotype is further consolidated by hsa-miR-363-3p and hsa-miR-223-3p (Figure 5B), which putatively target PTEN and TP53INP1, respectively, to prevent cell death and unleash metastatic potential (**PB1.4-3.2**) (26,52,53).

In this adaptive context, the profound downregulation of hsa-miR-200c emerges as a potentially critical event. As a potent guardian of the epithelial phenotype, its loss actively promotes cell motility, mesenchymal transition, and anoikis resistance by derepressing ZEB1/2 (54,55). Concurrently, the altered miRNA landscape in ulceration converges on the upregulation of central EMT inducers, including SNAIL2, TWIST, and HIF1A (**Cluster 2; Figure 5B; Figure S2B**). Dysregulation of these factors drives the repression of E-cadherin (**Cluster 7**) and the acquisition of mesenchymal traits essential for metastatic spread (4,40,56). Finally, while general Rho GTPase signaling supports survival during movement (**Clusters 1-3**), our data reveal a specific fine-tuning mechanism involving RHOB (**PB3.2**). Unlike other family members, RHOB functions as a motility-limiting tumor suppressor and a sensor of apoptotic stress; notably, we identify it as a direct target of the overexpressed hsa-miR-223-3p (Figure 5B). This suggests that the miRNA-mediated suppression of RHOB may relieve constraints on invasive behavior, allowing cells to evade stress-induced death while enhancing their invasive capacity (57). Collectively, these pathways illustrate how miRNA dysregulation coordinates a multi-layered response, from metabolic rescue to EMT, providing the plasticity required for metastasis.

Our study has certain limitations inherent to in silico analyses. However, we validated the clinical and methodological robustness of our overall meta-analytical pipeline by performing an orthogonal cross-validation of our severity signature against the independent InterMEL consortium dataset (19). This large-scale cohort evaluated miRNA associations with melanoma ulceration using targeted NanoString profiling, a platform entirely distinct from the microarrays comprising our meta-analysis. Notably, by restricting our comparative analysis to the 125 miRNAs assessed on both platforms, we identified 9

significant shared miRNAs that exhibited complete directional concordance. Consequently, by strictly adhering to PRISMA guidelines and demonstrating this cross-platform validation, the miRNA signatures identified herein represent a robust consensus profile. This provides supporting evidence that the identified regulatory hubs reflect biologically relevant alterations rather than artifacts of specific experimental setups.

In conclusion, our integrative analysis provides a comprehensive map of the miRNA alterations associated with melanoma diagnosis and ulceration. Beyond their biomarker utility, these signatures may hold significant therapeutic implications. The identification of the hsa-miR-142-5p/CDK6 axis suggests that patients with this specific dysregulation might benefit from CDK4/6 inhibitors (e.g., palbociclib) to restore senescence checkpoints. Furthermore, the upregulation of hsa-miR-223-3p in ulcerated tissues, which may suppress the RHOB/PTEN surveillance axis, alongside the unleashing of EGFR signaling via the loss of miR-489/499, highlights a high-risk subgroup. These patients, who may develop resistance to BRAF inhibitors due to alternative survival pathways, could potentially benefit from combination therapies targeting EGFR-driven survival networks (58).

MATERIALS & METHODS

Systematic review

A systematic review was conducted in rigorous compliance to the Preferred Reporting Items for Systematic Reviews and Meta-Analysis (PRISMA) guidelines (59). We performed a comprehensive search of the Gene Expression Omnibus (GEO) (60) and ArrayExpress (AE) (61) repositories using the search terms: “melanoma”, “microRNAs”, “microRNA”, and “miRNA”. Studies were filtered based on the following inclusion criteria: (i) organism: *Homo sapiens*; and (ii) dataset type: “Non-coding RNA profiling by array" or “expression profiling by array”. Conversely, studies were excluded if they met any of the following criteria: i) lack of focus on melanoma pathology; ii) absence of miRNA expression data; iii) use of non-human tissue samples; iv) limited sample size (n<12); v) experimental designs involving drug treatments or interventions; or vi) use of in vitro cell line models, ensuring the analysis focused exclusively on clinical tissue specimens.

Bioinformatic strategy for melanoma biomarkers identification

The integrative bioinformatics workflow (**Figure S3**) encompassed five key stages: i) data acquisition, preprocessing, and quality control; ii) study-specific differential expression analysis; iii) random-effects meta-analysis; iv) functional enrichment of miRNA targets; and v) regulatory network construction and clinical interpretation. All computational analyses were executed using the R programming language (62). Key packages included *limma* (63) for differential expression, *Biobase* (64) for data structures, *ggplot2* (65) for visualization, *dplyr* (66) and *stringr* (67)for data manipulation and *factoextra* (68) for multivariate data visualization.

Data acquisition and preprocessing

Raw data from selected studies were retrieved and analyzed individually to categorize samples into the defined biological scenarios: the diagnostic scenario (primary melanoma vs. benign nevi; four studies) and the prognostic scenario (ulcerated vs. non-ulcerated primary cutaneous melanoma; four studies). To ensure biological consistency, only Homo sapiens-specific miRNAs were retained. Preprocessing involved a rigorous quality control pipeline. We applied descriptive statistics and Principal Component Analysis (PCA) to assess the distribution of interest groups and identify potential outliers ("anomalous samples"), which were excluded to prevent skewing downstream analyses. Subsequently, intra-study normalization and standardization were applied to ensure data comparability, minimize batch effects, and reduce technical variability prior to the meta-analysis.

Differential expression and meta-analysis

Intra-study differential expression analysis was performed using linear models for microarray data implemented in the *limma* R package. Contrast matrices were constructed to compare the biological groups defined in the study design: Primary Melanoma vs. Benign Nevi (Diagnostic scenario) and Ulcerated vs. Non-Ulcerated Melanoma (Prognostic scenario). Subsequently, a random-effects meta-analysis was conducted for each scenario using the *metafor* package (69), applying the DerSimonian & Laird estimator (70). This approach addresses inter-study heterogeneity by weighting individual effect sizes by the inverse of their variance plus the between-study variance component. For each miRNA, we computed the combined log2 fold-change (logFC), standard error (SE), 95% confidence intervals (CI), and z-statistics. miRNAs with a Benjamini-Hochberg adjusted p-value < 0.05 (71) and an absolute logFC > 0.5 were considered significantly differentially expressed.

Functional characterization of miRNAs targets

To elucidate the biological implications of the miRNA signatures, we performed a Gene Set Analysis (GSA) based on experimentally validated targets. First, the complete list of meta-analyzed miRNAs was mapped to their target genes using the TarBase v8.0 (72) and miRTarBase v9.0 (73) databases, filtering for interactions with experimental evidence. Functional enrichment was assessed using the *mdgsa* R package (version 0.99.2) (74). Unlike standard over-representation analyses, this method employs a logistic regression model to transfer the differential expression signal (ranking index based on p-value and logFC) from miRNAs to their respective mRNA targets. Functional annotations were retrieved from the GO (75) Biological Process and REACTOME (76) databases using *biomaRt* (version 2.50.3) (77) and *Reactome.db* (version 1.77.0) (78), respectively. P-values adjusted using the Benjamini-Hochberg method < 0.05 were considered statistically significant. To prioritize the most biologically relevant processes, we applied an enrichment effect size cutoff (absolute log odds ratio) of > 0.5 for the diagnostic scenario. For the prognostic scenario, given the high density of dysregulated pathways, a stricter cutoff of > 0.75 was implemented to enhance specificity and minimize functional redundancy. Finally, to reduce complexity and visualize high-level functional modules, significant GO terms were clustered based on semantic similarity using the *simplifyEnrichment* package (version 1.10.0) (79) and REVIGO web-tool (80), utilizing the SimRel measure (similarity cutoff = 0.9). The resulting functional networks were visualized and refined using Cytoscape (version 3.10.1) (81).

miRNA-target gene interactions

To delineate the functional architecture of the identified signatures, we constructed interaction networks integrating significant miRNAs with their high-confidence target genes (**Table S11**). Target identification was performed using *miRTarBase v9.0*, applying a strict tripartite filtering strategy to ensure biological relevance and minimize false positives. This protocol prioritized targets supported by 'strong evidence' (e.g., luciferase reporter assays, Western blot, or qPCR), whereas targets supported only by 'less strong evidence' (e.g., HTP sequencing, microarrays) were retained solely if validated by at least three independent experimental methods. Furthermore, reflecting the cooperative nature of miRNA-mediated silencing, we selected hub genes subject to co-regulation by multiple differentially expressed miRNAs. Finally, to exclude non-physiological interactions, a tissue-expression filter was applied using the stringApp within Cytoscape, retaining only targets with a validated expression score of ≥2 (out of 5) in skin tissue.

Finally, two distinct network types were constructed and visualized using *Cytoscape* (version 3.10.1): i) Protein-Protein Interaction (PPI) Networks, based on the STRING database (confidence score > 0.4) to identify functional protein modules (clusters) disrupted by the miRNA signature; and ii) miRNA-Target Regulatory Networks, to map the specific hierarchical control of these modules by the dysregulated miRNAs.

CONFLICT OF INTEREST

All the authors declare no conflict of interest.

ACKNOWLEDGEMENTS

The authors thank the Principe Felipe Research Center (CIPF) for providing access to the cluster, co-funded by European Regional Development Funds (FEDER) in the Valencian Community 2014-2020. We would like to thank Dr Patricia P. Centeno of the Cancer Research UK Scotland Institute, for her guidance on this manuscript. The authors also thank Stuart P. Atkinson for reviewing the manuscript.

FUNDING

This research was supported by and partially funded by the Institute of Health Carlos III (project IMPaCT-Data, exp. IMP/00019), co-funded by the European Union, European Regional Development Fund (FEDER, "A way to make Europe"), and PID2021-124430OA-I00 funded by MCIN/AEI/10.13039/501100011033/ FEDER, UE ("A way to make Europe"). Borja Gómez-Cabañes is supported by a PhD fellowship funded by the Spanish Association Against Cancer in Valencia (PRDVA234163GOME). E.H. is supported by U54CA263001, R01CA274100 and P50CA225450 (National Cancer Institute, NCI/National Institutes of Health, NIH). N.M.E. was supported by F30CA288047 (NCI/NIH)

DATA AVAILABILITY

The data used for the analyses described in this work are publicly available at GEO and AE repositories (60,61). The accession numbers of the GEO datasets downloaded are GSE18509, GSE34460, GSE59334, GSE62370, GSE62371, GSE211090, and GSE211092. The accession number of the AE datasets downloaded is EMTAB4915.

AUTHOR CONTRIBUTIONS STATEMENT

Conceptualization: EH, FGG; Data Curation: HGM, BGC; Investigation: BGC, HGM, CGR, ZA, ALC, NME, JALG, EH, FGG; Supervision: EH, FGG, ALC; Writing-Original Draft Preparation: BGC, HGM, CGR, ZA, ALC, NME, JALG, EH, MRHG, FGG; all authors read and approved the final manuscript.

ORCiDs and email addresses:

Borja Gómez-Cabañes: https://orcid.org/0000-0002-1126-5667 (bgomezc@cipf.es)
Helena Gómez-Martínez: https://orcid.org/0000-0001-8714-5197 (hegomezmartinez@gmail.com)
Cristina Galiana-Roselló: https://orcid.org/0000-0003-1365-1323 (cgaliana@cipf.es)
Zoraida Andreu: https://orcid.org/0000-0002-7407-4825 (zandreu@fivo.org)
Adolfo López-Cerdán: https://orcid.org/0000-0001-9704-1877 (adlpecer@gmail.com)
Nicole M. Eskow: http://orcid.org/0000-0003-1048-4769 (Nicole.Eskow@nyulangone.org)
José A López-Guerrero: https://orcid.org/0000-0002-7369-8388 (jalopez@fivo.org)
Marta R. Hidalgo: https://orcid.org/0000-0002-5801-7804 (marta.hidalgo@uv.es)
Eva Hernando: https://orcid.org/0000-0003-1023-0312 (Eva.Hernando-Monge@nyulangone.org)
Francisco García-García: http://orcid.org/0000-0001-8354-5636 (fgarcia@cipf.es)

REFERENCES

1. Miller AJ, Mihm MC. Melanoma. N Engl J Med. 2006 Jul 6;355(1):51–65. doi:10.1056/NEJMra052166 PubMed PMID: 16822996.

2. Siegel RL, Miller KD, Fuchs HE, Jemal A. Cancer Statistics, 2021. CA Cancer J Clin. 2021 Jan;71(1):7–33. doi:10.3322/caac.21654 PubMed PMID: 33433946.

3. Siegel RL, Miller KD, Jemal A. Cancer statistics, 2016. CA Cancer J Clin. 2016;66(1):7–30. doi:10.3322/caac.21332 PubMed PMID: 26742998.

4. Pearlman RL, Montes de Oca MK, Pal HC, Afaq F. Potential therapeutic targets of epithelial-mesenchymal transition in melanoma. Cancer Lett. 2017 Apr 10;391:125–40. doi:10.1016/j.canlet.2017.01.029 PubMed PMID: 28131904; PubMed Central PMCID: PMC5371401.

5. Gershenwald JE, Scolyer RA, Hess KR, Sondak VK, Long GV, Ross MI, et al. Melanoma staging: Evidence-based changes in the American Joint Committee on Cancer eighth edition cancer staging manual. CA Cancer J Clin. 2017 Nov;67(6):472–92. doi:10.3322/caac.21409 PubMed PMID: 29028110; PubMed Central PMCID: PMC5978683.

6. Hayward NK, Wilmott JS, Waddell N, Johansson PA, Field MA, Nones K, et al. Whole-genome landscapes of major melanoma subtypes. Nature. 2017 May 11;545(7653):175–80. doi:10.1038/nature22071 PubMed PMID: 28467829.

7. Kirstein JM, Hague MN, McGowan PM, Tuck AB, Chambers AF. Primary melanoma tumor inhibits metastasis through alterations in systemic hemostasis. J Mol Med Berl Ger. 2016 Aug;94(8):899–910. doi:10.1007/s00109-016-1415-2 PubMed PMID: 27048169.

8. Komina A, Palkina N, Aksenenko M, Tsyrenzhapova S, Ruksha T. Antiproliferative and Pro-Apoptotic Effects of MiR-4286 Inhibition in Melanoma Cells. PloS One. 2016;11(12):e0168229. doi:10.1371/journal.pone.0168229 PubMed PMID: 28005927; PubMed Central PMCID: PMC5179095.

9. Naik PP. Cutaneous Malignant Melanoma: A Review of Early Diagnosis and Management. World J Oncol. 2021 Feb;12(1):7–19. doi:10.14740/wjon1349 PubMed PMID: 33738001; PubMed Central PMCID: PMC7935621.

10. Ghafouri-Fard S, Gholipour M, Taheri M. MicroRNA Signature in Melanoma: Biomarkers and Therapeutic Targets. Front Oncol. 2021 Apr 22;11:608987. doi:10.3389/fonc.2021.608987

11. Neagu M, Constantin C, Tanase C. Immune-related biomarkers for diagnosis/prognosis and therapy monitoring of cutaneous melanoma. Expert Rev Mol Diagn. 2010 Oct;10(7):897–919. doi:10.1586/erm.10.81 PubMed PMID: 20964610.

12. Nirschl CJ, Suárez-Fariñas M, Izar B, Prakadan S, Dannenfelser R, Tirosh I, et al. IFNγ-Dependent Tissue-Immune Homeostasis Is Co-opted in the Tumor Microenvironment. Cell. 2017 Jun 29;170(1):127-141.e15. doi:10.1016/j.cell.2017.06.016 PubMed PMID: 28666115; PubMed Central PMCID: PMC5569303.

13. O'Shea SJ, Rogers Z, Warburton F, Ramirez AJ, Newton-Bishop JA, Forbes LJL. Which symptoms are linked to a delayed presentation among melanoma patients? A retrospective study. BMC Cancer. 2017 Jan 3;17(1):5. doi:10.1186/s12885-016-2978-6 PubMed PMID: 28049453; PubMed Central PMCID: PMC5209829.

14. Sandru A, Voinea S, Panaitescu E, Blidaru A. Survival rates of patients with metastatic malignant melanoma. J Med Life. 2014;7(4):572–6. PubMed PMID: 25713625; PubMed Central PMCID: PMC4316142.

15. Mueller DW, Rehli M, Bosserhoff AK. miRNA expression profiling in melanocytes and melanoma cell lines reveals miRNAs associated with formation and progression of malignant melanoma. J Invest Dermatol. 2009 Jul;129(7):1740–51. doi:10.1038/jid.2008.452 PubMed PMID: 19212343.

16. Caramuta S, Egyházi S, Rodolfo M, Witten D, Hansson J, Larsson C, et al. MicroRNA expression profiles associated with mutational status and survival in malignant melanoma. J Invest Dermatol. 2010 Aug;130(8):2062–70. doi:10.1038/jid.2010.63 PubMed PMID: 20357817.

17. Mirzaei H, Naseri G, Rezaee R, Mohammadi M, Banikazemi Z, Mirzaei HR, et al. Curcumin: A new candidate for melanoma therapy? Int J Cancer. 2016 Oct 15;139(8):1683–95. doi:10.1002/ijc.30224 PubMed PMID: 27280688.

18. Page MJ, McKenzie JE, Bossuyt PM, Boutron I, Hoffmann TC, Mulrow CD, et al. The PRISMA 2020 statement: an updated guideline for reporting systematic reviews. BMJ. 2021 Mar 29;n71. doi:10.1136/bmj.n71

19. Wiggins JM, Zhang Q, Zhang Y, Vand-Rajabpour F, Hanniford D, He L, et al. Tumor miRNA Signatures Associate with Outcomes of Patients with Stage II/III Melanoma. Clin Cancer Res Off J Am Assoc Cancer Res. 2025 Dec 15;31(24):5225–36. doi:10.1158/1078-0432.CCR-24-3785 PubMed PMID: 41114662; PubMed Central PMCID: PMC12588674.

20. Chen J. The Cell-Cycle Arrest and Apoptotic Functions of p53 in Tumor Initiation and Progression. Cold Spring Harb Perspect Med. 2016 Mar 1;6(3):a026104. doi:10.1101/cshperspect.a026104 PubMed PMID: 26931810; PubMed Central PMCID: PMC4772082.

21. Miller DM, Flaherty KT. Cyclin-dependent kinases as therapeutic targets in melanoma. Pigment Cell Melanoma Res. 2014 May;27(3):351–65. doi:10.1111/pcmr.12211 PubMed PMID: 24405945.

22. Liu XL, Ding J, Meng LH. Oncogene-induced senescence: a double edged sword in cancer. Acta Pharmacol Sin. 2018 Oct;39(10):1553–8. doi:10.1038/aps.2017.198 PubMed PMID: 29620049; PubMed Central PMCID: PMC6289471.

23. Hoare M, Young ARJ, Narita M. Autophagy in cancer: having your cake and eating it. Semin Cancer Biol. 2011 Dec;21(6):397–404. doi:10.1016/j.semcancer.2011.09.004 PubMed PMID: 21945348.

24. Rodier F, Campisi J. Four faces of cellular senescence. J Cell Biol. 2011 Feb 21;192(4):547–56. doi:10.1083/jcb.201009094 PubMed PMID: 21321098; PubMed Central PMCID: PMC3044123.

25. Ritschka B, Storer M, Mas A, Heinzmann F, Ortells MC, Morton JP, et al. The senescence-associated secretory phenotype induces cellular plasticity and tissue regeneration. Genes Dev. 2017 Jan 15;31(2):172–83. doi:10.1101/gad.290635.116 PubMed PMID: 28143833; PubMed Central PMCID: PMC5322731.

26. Shahbazi J, Lock R, Liu T. Tumor Protein 53-Induced Nuclear Protein 1 Enhances p53 Function and Represses Tumorigenesis. Front Genet. 2013;4:80. doi:10.3389/fgene.2013.00080 PubMed PMID: 23717325; PubMed Central PMCID: PMC3652520.

27. Malekan M, Ebrahimzadeh MA, Sheida F. The role of Hypoxia-Inducible Factor-1alpha and its signaling in melanoma. Biomed Pharmacother Biomedecine Pharmacother. 2021 Sep;141:111873. doi:10.1016/j.biopha.2021.111873 PubMed PMID: 34225012.

28. Liu J, Zheng R, Zhang Y, Jia S, He Y, Liu J. The Cross Talk between Cellular Senescence and Melanoma: From Molecular Pathogenesis to Target Therapies. Cancers. 2023 May 6;15(9):2640. doi:10.3390/cancers15092640 PubMed PMID: 37174106; PubMed Central PMCID: PMC10177054.

29. Sheppard KE, McArthur GA. The cell-cycle regulator CDK4: an emerging therapeutic target in melanoma. Clin Cancer Res Off J Am Assoc Cancer Res. 2013 Oct 1;19(19):5320–8. doi:10.1158/1078-0432.CCR-13-0259 PubMed PMID: 24089445.

30. Garutti M, Targato G, Buriolla S, Palmero L, Minisini AM, Puglisi F. CDK4/6 Inhibitors in Melanoma: A Comprehensive Review. Cells. 2021 May 28;10(6):1334. doi:10.3390/cells10061334 PubMed PMID: 34071228; PubMed Central PMCID: PMC8227121.

31. Young AR, Narita M. Connecting autophagy to senescence in pathophysiology. Curr Opin Cell Biol. 2010 Apr;22(2):234–40. doi:10.1016/j.ceb.2009.12.005 PubMed PMID: 20045302.

32. Rao SG, Jackson JG. SASP: Tumor Suppressor or Promoter? Yes! Trends Cancer. 2016 Nov;2(11):676–87. doi:10.1016/j.trecan.2016.10.001

33. Zhang Y, Alexander PB, Wang XF. TGF-β Family Signaling in the Control of Cell Proliferation and Survival. Cold Spring Harb Perspect Biol. 2017 Apr 3;9(4):a022145. doi:10.1101/cshperspect.a022145 PubMed PMID: 27920038; PubMed Central PMCID: PMC5378054.

34. Batlle E, Massagué J. Transforming Growth Factor-β Signaling in Immunity and Cancer. Immunity. 2019 Apr 16;50(4):924–40. doi:10.1016/j.immuni.2019.03.024 PubMed PMID: 30995507; PubMed Central PMCID: PMC7507121.

35. Pickup MW, Owens P, Moses HL. TGF-β, Bone Morphogenetic Protein, and Activin Signaling and the Tumor Microenvironment. Cold Spring Harb Perspect Biol. 2017 May 1;9(5):a022285. doi:10.1101/cshperspect.a022285 PubMed PMID: 28062564; PubMed Central PMCID: PMC5411701.

36. Neagu M. Metabolic Traits in Cutaneous Melanoma. Front Oncol. 2020;10:851. doi:10.3389/fonc.2020.00851 PubMed PMID: 32509589; PubMed Central PMCID: PMC7248353.

37. Chen CY, Chen J, He L, Stiles BL. PTEN: Tumor Suppressor and Metabolic Regulator. Front Endocrinol. 2018;9:338. doi:10.3389/fendo.2018.00338 PubMed PMID: 30038596; PubMed Central PMCID: PMC6046409.

38. Wei Z, Xia J, Li J, Cai J, Shan J, Zhang C, et al. SIRT1 promotes glucolipid metabolic conversion to facilitate tumor development in colorectal carcinoma. Int J Biol Sci. 2023;19(6):1925–40. doi:10.7150/ijbs.76704 PubMed PMID: 37063423; PubMed Central PMCID: PMC10092765.

39. Ohanna M, Bonet C, Bille K, Allegra M, Davidson I, Bahadoran P, et al. SIRT1 promotes proliferation and inhibits the senescence-like phenotype in human melanoma cells. Oncotarget. 2014 Apr 30;5(8):2085–95. doi:10.18632/oncotarget.1791 PubMed PMID: 24742694; PubMed Central PMCID: PMC4039147.

40. Paoli P, Giannoni E, Chiarugi P. Anoikis molecular pathways and its role in cancer progression. Biochim Biophys Acta. 2013 Dec;1833(12):3481–98. doi:10.1016/j.bbamcr.2013.06.026 PubMed PMID: 23830918.

41. Hao Y, Baker D, Ten Dijke P. TGF-β-Mediated Epithelial-Mesenchymal Transition and Cancer Metastasis. Int J Mol Sci. 2019 Jun 5;20(11):2767. doi:10.3390/ijms20112767 PubMed PMID: 31195692; PubMed Central PMCID: PMC6600375.

42. Han M, Liu M, Wang Y, Mo Z, Bi X, Liu Z, et al. Re-expression of miR-21 contributes to migration and invasion by inducing epithelial-mesenchymal transition consistent with cancer stem cell characteristics in MCF-7 cells. Mol Cell Biochem. 2012 Apr;363(1–2):427–36. doi:10.1007/s11010-011-1195-5 PubMed PMID: 22187223.

43. Liu LZ, Li C, Chen Q, Jing Y, Carpenter R, Jiang Y, et al. MiR-21 induced angiogenesis through AKT and ERK activation and HIF-1α expression. PloS One. 2011 Apr 22;6(4):e19139. doi:10.1371/journal.pone.0019139 PubMed PMID: 21544242; PubMed Central PMCID: PMC3081346.

44. Schafer ZT, Grassian AR, Song L, Jiang Z, Gerhart-Hines Z, Irie HY, et al. Antioxidant and oncogene rescue of metabolic defects caused by loss of matrix attachment. Nature. 2009 Sep 3;461(7260):109–13. doi:10.1038/nature08268 PubMed PMID: 19693011; PubMed Central PMCID: PMC2931797.

45. Endo H, Owada S, Inagaki Y, Shida Y, Tatemichi M. Metabolic reprogramming sustains cancer cell survival following extracellular matrix detachment. Redox Biol. 2020 Sep;36:101643. doi:10.1016/j.redox.2020.101643 PubMed PMID: 32863227; PubMed Central PMCID: PMC7371916.

46. Taddei ML, Giannoni E, Fiaschi T, Chiarugi P. Anoikis: an emerging hallmark in health and diseases. J Pathol. 2012 Jan;226(2):380–93. doi:10.1002/path.3000 PubMed PMID: 21953325.

47. Giannoni E, Bianchini F, Calorini L, Chiarugi P. Cancer associated fibroblasts exploit reactive oxygen species through a proinflammatory signature leading to epithelial mesenchymal transition and stemness. Antioxid Redox Signal. 2011 Jun 15;14(12):2361–71. doi:10.1089/ars.2010.3727 PubMed PMID: 21235356.

48. Avivar-Valderas A, Salas E, Bobrovnikova-Marjon E, Diehl JA, Nagi C, Debnath J, et al. PERK integrates autophagy and oxidative stress responses to promote survival during extracellular matrix detachment. Mol Cell Biol. 2011 Sep;31(17):3616–29. doi:10.1128/MCB.05164-11 PubMed PMID: 21709020; PubMed Central PMCID: PMC3165554.

49. Zhang Y hong, Wu Y liang, Tashiro S ichi, Onodera S, Ikejima T. Reactive oxygen species contribute to oridonin-induced apoptosis and autophagy in human cervical carcinoma HeLa cells. Acta Pharmacol Sin. 2011 Oct;32(10):1266–75. doi:10.1038/aps.2011.92 PubMed PMID: 21892202; PubMed Central PMCID: PMC4010075.

50. Whelan KA, Caldwell SA, Shahriari KS, Jackson SR, Franchetti LD, Johannes GJ, et al. Hypoxia suppression of Bim and Bmf blocks anoikis and luminal clearing during mammary morphogenesis. Mol Biol Cell. 2010 Nov 15;21(22):3829–37. doi:10.1091/mbc.E10-04-0353 PubMed PMID: 20861305; PubMed Central PMCID: PMC2982135.

51. Reginato MJ, Mills KR, Paulus JK, Lynch DK, Sgroi DC, Debnath J, et al. Integrins and EGFR coordinately regulate the pro-apoptotic protein Bim to prevent anoikis. Nat Cell Biol. 2003 Aug;5(8):733–40. doi:10.1038/ncb1026 PubMed PMID: 12844146.

52. Zilfou JT, Lowe SW. Tumor suppressive functions of p53. Cold Spring Harb Perspect Biol. 2009 Nov;1(5):a001883. doi:10.1101/cshperspect.a001883 PubMed PMID: 20066118; PubMed Central PMCID: PMC2773645.

53. Vitolo MI, Weiss MB, Szmacinski M, Tahir K, Waldman T, Park BH, et al. Deletion of PTEN promotes tumorigenic signaling, resistance to anoikis, and altered response to chemotherapeutic agents in human mammary epithelial cells. Cancer Res. 2009 Nov 1;69(21):8275–83. doi:10.1158/0008-5472.CAN-09-1067 PubMed PMID: 19843859; PubMed Central PMCID: PMC2783190.

54. Tryndyak VP, Beland FA, Pogribny IP. E-cadherin transcriptional down-regulation by epigenetic and microRNA-200 family alterations is related to mesenchymal and drug-resistant phenotypes in human breast cancer cells. Int J Cancer. 2010 Jun 1;126(11):2575–83. doi:10.1002/ijc.24972 PubMed PMID: 19839049.

55. Howe EN, Cochrane DR, Richer JK. Targets of miR-200c mediate suppression of cell motility and anoikis resistance. Breast Cancer Res BCR. 2011 Apr 18;13(2):R45. doi:10.1186/bcr2867 PubMed PMID: 21501518; PubMed Central PMCID: PMC3219208.

56. Dongre A, Weinberg RA. New insights into the mechanisms of epithelial–mesenchymal transition and implications for cancer. Nat Rev Mol Cell Biol. 2019 Feb;20(2):69–84. doi:10.1038/s41580-018-0080-4

57. Zaoui K, Duhamel S. RhoB as a tumor suppressor: It's all about localization. Eur J Cell Biol. 2023 Jun;102(2):151313. doi:10.1016/j.ejcb.2023.151313 PubMed PMID: 36996579.

58. Sun C, Wang L, Huang S, Heynen GJJE, Prahallad A, Robert C, et al. Reversible and adaptive resistance to BRAF(V600E) inhibition in melanoma. Nature. 2014 Apr 3;508(7494):118–22. doi:10.1038/nature13121 PubMed PMID: 24670642.

59. Moher D, Liberati A, Tetzlaff J, Altman DG, PRISMA Group. Preferred reporting items for systematic reviews and meta-analyses: the PRISMA statement. PLoS Med. 2009 Jul 21;6(7):e1000097. doi:10.1371/journal.pmed.1000097 PubMed PMID: 19621072; PubMed Central PMCID: PMC2707599.

60. Edgar R, Domrachev M, Lash AE. Gene Expression Omnibus: NCBI gene expression and hybridization array data repository. Nucleic Acids Res. 2002 Jan 1;30(1):207–10. doi:10.1093/nar/30.1.207 PubMed PMID: 11752295; PubMed Central PMCID: PMC99122.

61. Parkinson H, Kapushesky M, Shojatalab M, Abeygunawardena N, Coulson R, Farne A, et al. ArrayExpress--a public database of microarray experiments and gene expression profiles. Nucleic Acids Res. 2007 Jan;35(Database issue):D747-750. doi:10.1093/nar/gkl995 PubMed PMID: 17132828; PubMed Central PMCID: PMC1716725.

62. R Core Team. R: A language and environment for statistical computing [Internet]. Vienna, Austria: R Foundation for Statistical Computing; 2025. Available from: https://www.R-project.org/

63. Ritchie ME, Phipson B, Wu D, Hu Y, Law CW, Shi W, et al. limma powers differential expression analyses for RNA-sequencing and microarray studies. Nucleic Acids Res. 2015 Apr 20;43(7):e47. doi:10.1093/nar/gkv007 PubMed PMID: 25605792; PubMed Central PMCID: PMC4402510.

64. Huber W, Carey VJ, Gentleman R, Anders S, Carlson M, Carvalho BS, et al. Orchestrating high-throughput genomic analysis with Bioconductor. Nat Methods. 2015 Feb;12(2):115–21. doi:10.1038/nmeth.3252 PubMed PMID: 25633503; PubMed Central PMCID: PMC4509590.

65. Wickham H. ggplot2: elegant graphics for data analysis. Second edition. Cham: Springer international publishing; 2016. 1 p. (Use R!).

66. Wickham H, François R, Henry L, Müller K, Vaughan D. dplyr: A Grammar of Data Manipulation [Internet]. Available from: https://dplyr.tidyverse.org

67. Wickham H. stringr: Simple, Consistent Wrappers for Common String Operations [Internet]. 2025. Available from: https://stringr.tidyverse.org

68. Kassambara A, Mundt F. factoextra: Extract and Visualize the Results of Multivariate Data Analyses [Internet]. Available from: http://www.sthda.com/english/rpkgs/factoextra

69. Viechtbauer W. Conducting Meta-Analyses in *R* with the **metafor** Package. J Stat Softw. 2010;36(3). doi:10.18637/jss.v036.i03

70. DerSimonian R, Laird N. Meta-analysis in clinical trials. Control Clin Trials. 1986 Sep;7(3):177–88. doi:10.1016/0197-2456(86)90046-2 PubMed PMID: 3802833.

71. Benjamini Y, Drai D, Elmer G, Kafkafi N, Golani I. Controlling the false discovery rate in behavior genetics research. Behav Brain Res. 2001 Nov 1;125(1–2):279–84. doi:10.1016/s0166-4328(01)00297-2 PubMed PMID: 11682119.

72. Skoufos G, Kakoulidis P, Tastsoglou S, Zacharopoulou E, Kotsira V, Miliotis M, et al. TarBase-v9.0 extends experimentally supported miRNA-gene interactions to cell-types and virally encoded miRNAs. Nucleic Acids Res. 2024 Jan 5;52(D1):D304–10. doi:10.1093/nar/gkad1071 PubMed PMID: 37986224; PubMed Central PMCID: PMC10767993.

73. Huang HY, Lin YCD, Cui S, Huang Y, Tang Y, Xu J, et al. miRTarBase update 2022: an informative resource for experimentally validated miRNA-target interactions. Nucleic Acids Res. 2022 Jan 7;50(D1):D222–30. doi:10.1093/nar/gkab1079 PubMed PMID: 34850920; PubMed Central PMCID: PMC8728135.

74. Montaner D, Dopazo J. Multidimensional gene set analysis of genomic data. PloS One. 2010 Apr 27;5(4):e10348. doi:10.1371/journal.pone.0010348 PubMed PMID: 20436964; PubMed Central PMCID: PMC2860497.

75. Gene Ontology Consortium, Aleksander SA, Balhoff J, Carbon S, Cherry JM, Drabkin HJ, et al. The Gene Ontology knowledgebase in 2023. Genetics. 2023 May 4;224(1):iyad031. doi:10.1093/genetics/iyad031 PubMed PMID: 36866529; PubMed Central PMCID: PMC10158837.

76. Milacic M, Beavers D, Conley P, Gong C, Gillespie M, Griss J, et al. The Reactome Pathway Knowledgebase 2024. Nucleic Acids Res. 2024 Jan 5;52(D1):D672–8. doi:10.1093/nar/gkad1025 PubMed PMID: 37941124; PubMed Central PMCID: PMC10767911.

77. Durinck S, Moreau Y, Kasprzyk A, Davis S, De Moor B, Brazma A, et al. BioMart and Bioconductor: a powerful link between biological databases and microarray data analysis. Bioinformatics. 2005 Aug 15;21(16):3439–40. doi:10.1093/bioinformatics/bti525 PubMed PMID: 16082012.

78. Ligtenberg W. reactome.db: A set of annotation maps for reactome.

79. Gu Z, Hübschmann D. simplifyEnrichment: A Bioconductor Package for Clustering and Visualizing Functional Enrichment Results. Genomics Proteomics Bioinformatics. 2023 Feb;21(1):190–202. doi:10.1016/j.gpb.2022.04.008 PubMed PMID: 35680096; PubMed Central PMCID: PMC10373083.

80. Supek F, Bošnjak M, Škunca N, Šmuc T. REVIGO summarizes and visualizes long lists of gene ontology terms. PloS One. 2011;6(7):e21800. doi:10.1371/journal.pone.0021800 PubMed PMID: 21789182; PubMed Central PMCID: PMC3138752.

81. Shannon P, Markiel A, Ozier O, Baliga NS, Wang JT, Ramage D, et al. Cytoscape: a software environment for integrated models of biomolecular interaction networks. Genome Res. 2003 Nov;13(11):2498–504. doi:10.1101/gr.1239303 PubMed PMID: 14597658; PubMed Central PMCID: PMC403769.